EPH - International Journal of Applied Science

ISSN (Online): 2208-2182
Volume 5 Issue 02 June-2019

DOI: https://doi.org/10.53555/eijas.v5i2.118

PHYSICOCHEMICAL CHARACTERISTICS AND PROPERTIES OF NANO-MODIFIED COUPLED SMECTITE CATALYSTS WITH AG^{+}/ZN^{2+}

Shu-Lung Kuo[1], Edward Ming-Yang Wu[2*]
[1]Department of Technology Management, the Open University of Kaohsiung, Taiwan
*[*2] Department of Civil and Ecological Engineering, I-Shou University, Kaohsiung, Taiwan*

Corresponding Author:-

Abstract:-

This study used smectite clay as a carrier and exchanged Ag^{+} and Zn^{2+} onto the smectite via ion exchange. The coupled smectite-Ag/Zn catalysts at the nanolevel were formed after surface modification and high-temperature sintering. Various physicochemical experiments, such as Fourier-transform infrared spectroscopy (FT-IR) analysis, x-ray diffraction (XRD) analysis, transmission electron microscopy (TEM) analysis, and thermal analysis, were conducted to further discuss the physicochemical properties of the smectite-Ag/Zn.

A function group analysis on the modified coupled smectite-Ag/Zn catalysts conducted via an FT-IR spectrum shows that the mineral structures of the catalysts remain intact after high-temperature sintering. In terms of the x-ray analysis, water tends to exist in the layer structure of the smectite, which is affected by humidity in the environment. After being modified by Ag and Zn, shrinkage occurs in layers of the smectite due to water loss. The spacing of layers is thereby narrowed. Moreover, a TEM observation of the coupled smectite-Ag/Zn catalysts after it was sintered at 350°C shows that the sizes of Ag^{+} and Zn^{+2} on the smectite-Ag/Zn are between 25-50 nm, respectively. This proves that Ag^{+} and Zn^{2+} do exist in the coupled smectite-Ag/Zn catalysts after they were exchanged, and that they are at the nanolevel. As for the thermal analysis, the findings show that significant melting occurs when the coupled smectite-Ag/Zn catalysts are sintered at 459°C, due to the oxidative pyrolysis of micromolecules or solvents.

Key words:-*Smectite, coupled catalysts, FT-IR, TEM analysis, thermal analysis*

1. INTRODUCTION

As one of the most promising methods to treat antibiotic contaminants, photocatalysis has attracted tremendous attention because it is an economic, efficient, and green technology for degrading antibiotics using sunlight and ambient conditions (Boxi and Paria, 2015; Kushwaha et al., 2015). Though the basic mechanism for photocatalytic degradation of antibiotics is similar to that of the degradation of organic dyes, most antibiotics are resistant to decomposition owing to their robust molecular structures. Hence, designing and fabricating appropriate photocatalysts with high photocatalytic activities requires considerable research. Among the diverse researched photocatalysts, TiO_2 has been the most studied semiconductor for photocatalysis since it was used as a photocatalyst by Fujishima and Honda in 1972 (Fujishima and Honda, 1972). Though much work has been directed towards enhancing the photocatalytic performance of TiO_2 via size and crystal face adjustments and morphology regulation, its application remains limited because of its restricted light absorption capability to the UV light region only (Satoh etal., 2008; Yang et al., 2008; Gordan et al., 2012; Xie et al., 2016). The latter corresponds to only about 4% of the solar light spectrum. Thus, to better exploit the solar light spectrum, it is highly desirable to develop and synthesise advanced photocatalyst systems, with enhanced photocatalytic activities, that can also be activated by visible-light irradiation (Pelaez et al., 2012).

During the last decade, photocatalyses are becoming more popular to draw significant global interest (Chen et al., 2009). Titanium dioxide (TiO_2) is the most widely used catalyst; it is considered to be an ideal catalyst for photocatalytic oxidation applications (Mo et al., 2009; Chen et al., 2010; Paz, 2010; Zhong et al., 2010). Numerous reports on the mechanisms of photocatalytic process for disinfecting air have been published in literature (Salvad-Estivilletal., 2007; Mo et al., 2009; Chen et al., 2010). However, not much research has been carried out on the photocatalytic disinfection of airborne bacteria in polluted indoor air despite its capacity and great potential to protect public health.

The main research approach is to use commercially available smectite as a catalyst carrier, and exchange Ag^+ and Zn^{2+} onto the catalyst carrier to form the so-called coupled smectite-Ag/Zn catalysts. The Fourier-transform infrared spectrometer (FTIR), x-ray diffractometer (XRD), transmission electron microscope (TEM), differential thermal scanning calorimeter (DSC), and thermogravimetric analyzer (TGA) are used to explore and verify various physical and chemical properties of the coupled smectite-Ag/Zn catalysts.

2. Materials and methods

2.1 Purification and preparation of sodium saturated smectite

Put 60 g commercially available smectite into a 2-liter beaker, and add 1.8 liters of deionized water to it. After stirring, soak it for days to fully expand it. After it is expanded, take 250 ml of the smectite suspension out of the beaker. Filter sand using the wet sieving method with a 300-mesh sieve. Transfer the filtrate to a 1-liter sedimentation cylinder, and add deionized water to make 1 liter. Leave it to naturally sediment after stirring it rigorously with a stirring rod. Siphon the suspension at the top of the sedimentation cylinder by 10 cm 8 hours later. Use an 18000 rpm high-speed centrifuge to have the suspension centrifuged. Perform sodium saturation of the smectite obtained after centrifugation with 1 M NaCl solution. Next, grind the saturated smectite into powder with an agate mortar after freeze drying it, and obtain the sodium saturated smectite.

2.2 Preparation of the coupled smectite-Ag/Zn catalysts

Formulate 58 ml of 0.1 N $AgNO_3$ and 42 ml of 0.1 N $ZnCl_2$, respectively. Add 2% of sodium saturated smectite and stir it for 48 hours using the water bath method, which keeps the temperature at 40°C. Next, stir it evenly for 2 hours at 80°C. Leave it and remove the supernatant. Use 50% ethanol to remove the chlorine ions. Dry the modified smectite-Ag/Zn catalysts using the freeze drying method. After taking them out and grinding them, sinter them in a high-temperature furnace at 350°C for 2 hours. Save them for later use when their temperature is lowered to room temperature. The concentrations of Ag and Zn in the prepared catalysts are the same.

2.3 An analysis of the properties of the smectite-Ag/Zn catalysts

2.3.1 Verification of the function group of Fourier-transform infrared spectroscopy (FT-IR)

The principle of FT-IR is using rotations or vibrations of molecules to absorb radiation at the same frequency. The fingerprint and Eigen areas in FT-IR can help to determine the existence of isomorphous replacement structure or organic molecules in the smectite-Ag/Zn catalysts.

Put the smectite-Ag/Zn and KBr powders in an oven. After heating them up and drying them for 48 hours, mix them evenly in a 1:10 ratio, and then grind the mixture with an agate mortar. Use a hydraulic press to press the mixture at 10 tons/hour, making it into a transparent foil. Put the foil in a spectrometer and perform an analysis with a scan range of 4,000 cm^{-1} to 400 cm^{-1}.

2.3.2 X-ray Diffraction Analysis (XRD Analysis)

The XRD analysis is conducted using an x-ray diffractometer (Rigaku RINT-2000). With CuK_a as the light source, an analysis on the crystal patterns of the smectite and smectite-Ag/Zn is performed to learn the spacing of layers of materials. The x-ray *O* wavelength produced is 1.5418 *A*; the operating current during testing is 10 mA; the voltage is 20 kV; the scanning speed is 5 deg/min; and the scanning angle is $2\theta=2\sim40^o$.

2.3.3 Transmission Electron Microscopy (TEM) Analysis

This study uses a transmission electron microscope to observe the particle size and distribution pattern of smectite-Ag/Zn catalysts. The model used is HR-TEM 2100. The steps for preparing samples to be tested are as follows: Take 0.1 g of

the smectite-Ag/Zn catalysts and put them in a centrifuge tube. Next, add 50% of alcohol (approximately 10 ml) to the tube. Put the tube in a beaker with water, and then oscillate it in an oscillator for approximately 30 minutes. Afterwards, use a Formvar carbon support film on grids with anti-static tweezers to collect the needed samples from the suspension in the tube; repeat this step twice. An analysis on the samples can be conducted after leaving them to stand.

2.3.4 Thermal analysis

This study uses the differential scanning calorimeter – thermogravimetric analyzer (DSC-TGA) to perform a thermal analysis on the smectite-Ag/Zn catalysts based on different temperature rising speeds. The brand of the instrument used is American TA Instruments. This instrument can be used to test changes in solid, powder, colloid and liquid materials at high temperatures. The analysis steps are as follows:

(1)Sample preparation: Fully dry the smectite-Ag/Zn catalysts to be tested after grinding them into fine powder with an agate mortar. Take 5-20 mg of the sample and put it on a platinum plate for testing.

(2)Analysis conditions: Use nitrogen as the purge gas with the temperature rising at 10°C/min. The scope of temperatures for scanning is between 40°C and 1200°C; the thermal stability, differential thermal curves, and weight loss of the sample will be measured.

3. Results and discussion

3.1 Results of FT-IR analysis

Figures 1 and 2 show the infrared spectroscopy analysis results of the smectite and smectite-Ag/Zn catalysts, respectively. Figure 1 shows many significant and complex wave crests in the following wavenumber sections in the fingerprint area: 415~600 cm^{1} and 750~1170 cm^{-1}; they represent strong bonds between impure silicates (Si-O) and silicates (O-Si-O) within the silicate mineral. Since a part of Si^{4+} within the silicates layer (tetrahedral layer) is replaced by Al^{3+} and many metal ions within the metal ion layer (octahedral layer) can go into the metal ion layer, various absorption characteristics of the octahedron's OH bending vibrations will be formed. If the octahedron contains aluminum only, its absorption peak is approximately 920 cm^{-1}; if it contains iron only, its absorption peak is approximately 820 cm^{-1}; if it contains both iron and magnesium, its absorption peak is approximately between 820~920 cm^{-1}. A further interpretation of the absorption area suggests that a split and shift occurs in the OH absorption peak between 3200 cm^{-1}~3700 cm^{-1}; the silicon within the tetrahedron will also be replaced by aluminum.

Figure 2 shows that the structure of said coupled catalysts remains intact after being sintered at 350°C for 2 hours; it still keeps the absorption band of clay minerals with inherent characteristics. As such, a catalyst carrier will still have a good clay structure via complex modification and sintering, whereby it can be used as a photocatalyst.

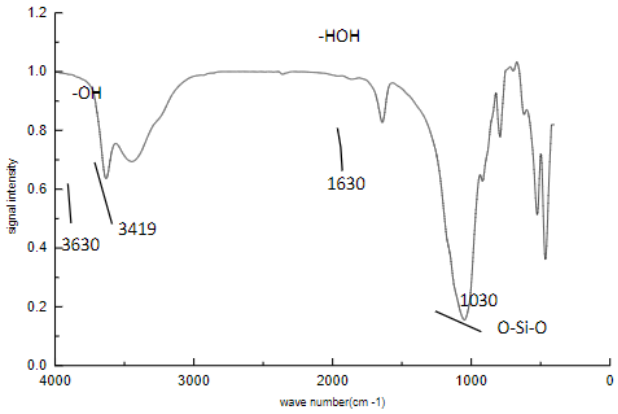

Figure 1. FT-IR spectrum of the smectite (before being sintered at high temperatures)

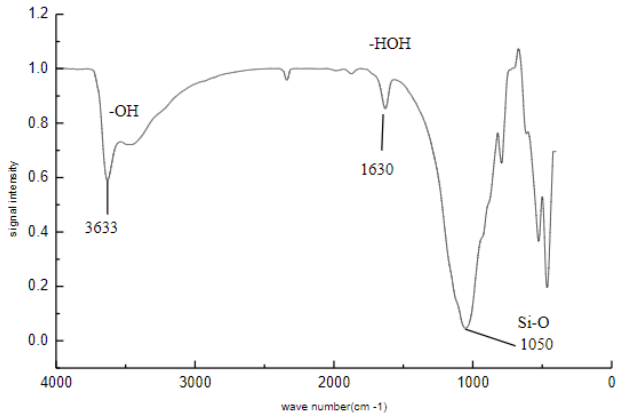

Figure 2. FT-IR spectrum of the smectite-Ag/Zn (sintered at 350°C)

3.2 Results of XRD analysis

Figure 3 shows the XRD analysis results of the sodium saturated smectite that was not sintered. Smectite is itself a layered structure; its layers are tightly bonded by the van der waals force. There are exchangeable positive ions between these layers. As such, we can exchange various positive ions with the sodium ions between layers of the smectite to achieve the objective of absorption equilibrium. Before the smectite was modified, the diffraction angle is $2\theta=6.91^{o}$ for the crystallographic plane of the regularly arranged silicates layer (001). According to Bragg's law: $2d\sin\theta=n\lambda$; the first diffraction peak is n=1, and λ is the wavelength of copper-palladium materials (1.5405 *A*). This result shows that the spacing of layers of the sodium saturated smectite at room temperature is 1.2782 nm.

Figure 4 shows the XRD analysis results of the smectite-Ag/Zn after being sintered at 350°C. Before the smectite was modified, the diffraction angle was $2\theta=6.91^{o}$ for the crystallographic plane of the regularly arranged silicates layer (001). According to Bragg's law: $2d\sin\theta=n\lambda$; the first diffraction peak is n=1, and λ is the wavelength of copper-palladium materials (1.5405 *A*). This result shows that the spacing of layers of the sodium saturated smectite at room temperature is 1.2782 nm. After being modified with Ag^{+} and Zn^{2+} and sintered at 350°C, the spacing of layers of the smectite-Ag/Zn narrows to 1.2701 nm, as shown in Figure 4. The smectite is a 2:1 expansion type clay mineral; water tends to exist in its layer structure if it is affected by humidity in the environment. After being modified by various metal-related positive ions, shrinkage occurs in its layers due to water loss. As such, the spacing of layers is narrowed.

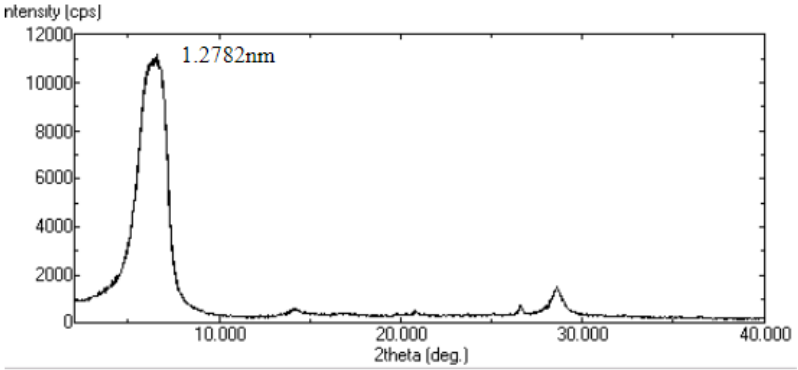

Figure 3. XRD analysis of the smectite (before being sintered at high temperatures)

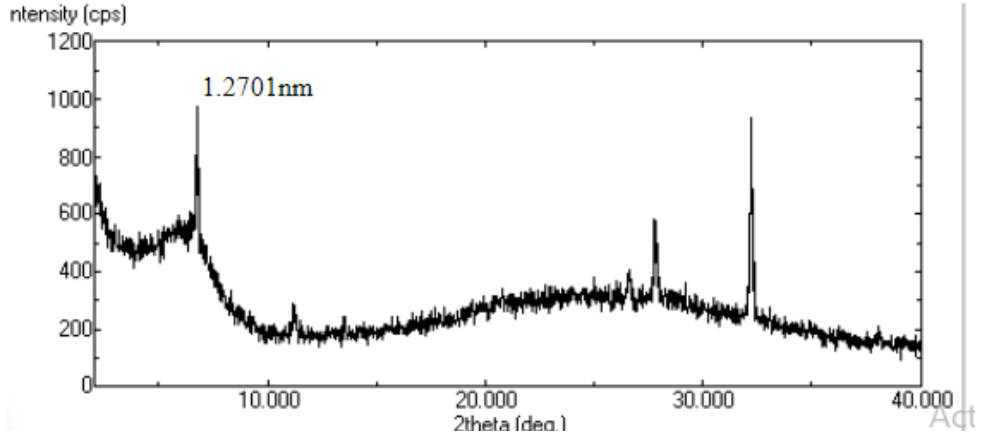

Figure 4. XRD analysis of the smectite-Ag/Zn (sintered at 350°C)

3.3 Results of TEM analysis

Figures 5(a) and 5(b) show the structural patterns of the smectite before being sintered. In Figure 5(a), the crystal lattice of the smectite that resembles fingerprints is quite intact. Also, since the smectite is an expansion type clay mineral, its surface structure is shown in 5(b) as a loosely layered pattern that resembles the shape of cotton. With the characteristic of a large surface area; using surfactants, it is suitable to be modified into organoclay with hydrophobic properties, while acting as the optimal carrier for catalysts. Figure 5(c) shows the modified smectite-Ag/Zn; those bigger granules in dark black are silver ions, and the light-colored ones are zinc ions. Their distributions are quite intensive. The above TEM analysis results verify that the spacing of distributions of ions within various smectite catalysts after synthesis is indeed at the nanolevel. Figure 6 shows the distribution of the smectite-Ag/Zn elements identified via an energy dispersive spectrometer (EDS). The Ag^{+} and Zn^{+2} contents in the smectite-Ag/Zn show certain proportions, indicating that the modified smectite-Ag/Zn indeed has the characteristics of coupled catalysts at the nanolevel.

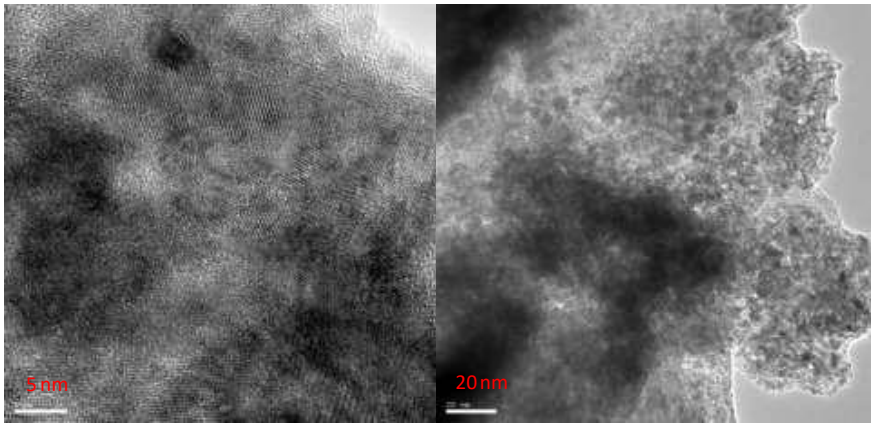

(a) Smectite **(b) smectite**

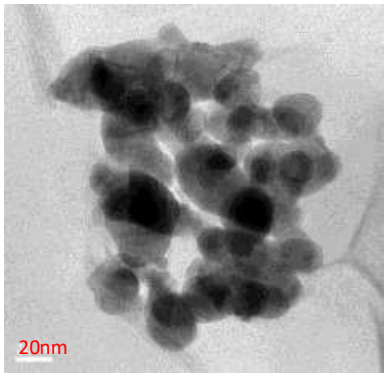

(c) smectite-Ag/Zn

Figure 5. TEM analysis of the smectite and smectite-Ag/Zn

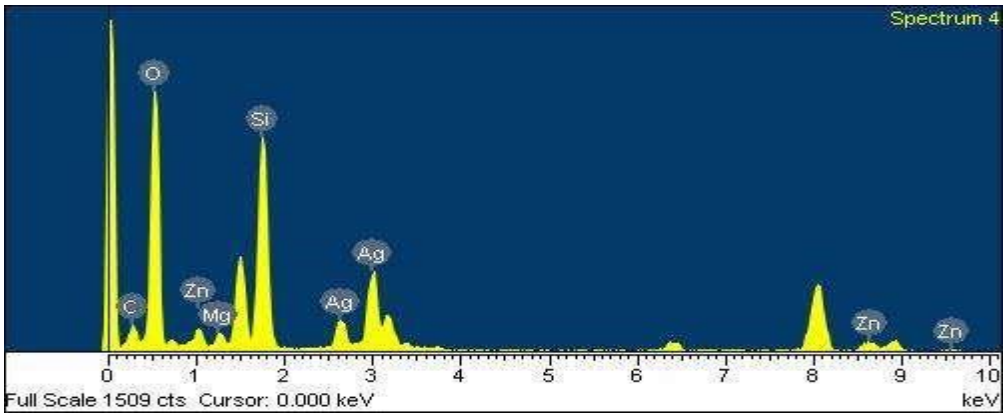

Figure 6. EDS analysis results of the smectite-Ag/Zn

3.4 Result of thermal analysis

Figures 7 and 8 show the results of an analysis on the smectite and smectite-Ag/Zn with the temperature rising at 10°C/min (from 40°C to 1200°C) conducted using a differential thermal scanning calorimeter, thermogravimetric analyzer (DSC-TGA) in a nitrogen atmosphere.

As illustrated by the thermal curves obtained from the differential thermal scanning calorimetry in Figure 7, the smectite has endothermic peaks (melting peaks) at 89°C, 700°C, 920°C, and 1057°C, respectively; it has exothermic peaks at 734°C and 950°C, respectively. In terms of having an endothermic peak at 700°C (Sobana et al., 2008), hydrate is produced from the smectite because of the high temperature, but no significant amorphous phenomenon occurs. Although it loses structural hydroxy, it maintains a framework with layered structure. However, the structure is twisted, whereby the characteristics of the smectite have been slightly lost. The TGA weight loss, as shown in the figure, is approximately 1.9%, which is very close to that described in literature (1.97%). The occurrence of the third and fourth endothermic peaks of the smectite suggests the dissolution of its structure; at this time, it is shown in amorphous form. In regard to TGA weight loss, two pyrolysis temperatures are found in the figure:

The first pyrolysis occurs at 135°C, where the weight loss is due to the decrease in the weight of micromolecules or solvents caused by oxidative pyrolysis. The second pyrolysis occurs at 607°C, where the TGA weight loss is due to the decomposition of the remaining organic (carbon-containing) compounds. During the first pyrolysis, the TGA weight loss from 135°C to 607°C is estimated to be about 3.2%. During the second pyrolysis, the TGA weight loss from 607°C to 706°C is estimated to be about 2.9%. Since smectite clay minerals are inorganic substances, they won't be burned down at high temperatures. However, most organic substances will be burned down at high temperatures. Overall, the weight

loss is not much. Moreover, there are two interpretations for the multiple melting phenomena of the smectite: First, the smectite itself has various crystal structures or micro-phase patterns. As such, these various crystals and phase patterns will reflect different melting peaks during the heating and melting process. Second, some unstable crystals of the smectite itself will melt at a lower temperature during the heating and melting process; they will then form more perfect crystals. These more perfect crystals will melt again when the temperature keeps rising, eventually forming multiple melting peaks. The exothermic peak at 734°C is probably caused by the effect of the smectite itself. This temperature (706°C) is the endpoint of the major weight loss. After this, the increase in weight loss slows down. Figure 7 shows 4 endothermic peaks, among which 3 are at higher temperatures. The reason behind this phenomenon is that the crystal structure of the smectite is relatively complete; only at a higher temperature can it melt. In other words, crystals formed at a lower temperature are more incomplete. Thus, they tend to undergo a continuous melting, recrystallization, and remelting process when temperatures continue to rise. This continuous process can be easily formed when the weight loss of the smectite slows down as it is at a high temperature. There will be endothermic peaks at 920°C and 1057°C, respectively (Sobana et al., 2008), which means that the smectite is in the dissolving, not the amorphous, state.

In terms of the smectite-Ag/Zn, Figure 8 shows endothermic peaks at 73°C, 459°C, 677°C and 1042°C, respectively; there are exothermic peaks at 478°C, 704°C and 1000°C, respectively. In regard to TGA weight loss, two pyrolysis temperatures are found in the figure: The first pyrolysis occurs at 478°C, where the weight loss is due to the decrease in the weight of micromolecules or solvents caused by oxidative pyrolysis. The second pyrolysis occurs at 799°C, where the TGA weight loss is due to the decomposition of the remaining organic (carbon-containing) compounds. During the first pyrolysis, the TGA weight loss from 478°C to 799°C is estimated to be about 4.5%. During the second pyrolysis, the TGA weight loss from 799°C to 998°C is estimated to be about 7.7%. The weight loss during the second pyrolysis is higher than that during the first pyrolysis, which shows that the original crystallization characteristics of the smectite have changed in the smectite-Ag/Zn; the increase in the speed of the weight loss of the organic (carbon-containing) compounds at the second pyrolysis temperature is due to a temperature rise (Zhang et al., 2009). Moreover, the exothermic peak at 1000°C before the endothermic peak at 1042°C and the surrounding endothermic peaks are less obvious. In other words, melting and recrystallization do not occur. On the other hand, the exothermic peak at 704°C and the endothermic peak at 677°C occur earlier than those for the smectite. A quite obvious endothermic peak occurs at 459°C; this timing is very close to that when the first pyrolysis temperature occurs. It can be inferred from this phenomenon that significant melting occurs when the coupled smectiteAg/Zn catalysts are sintered at 459°C, due to the oxidative pyrolysis of micromolecules or solvents; weight loss at this timing is quite obvious. By the second pyrolysis, when the temperature reaches 998°C, weight loss also seems to be quite obvious, since the exothermic peak and melting and recrystallization phenomena are less obvious.

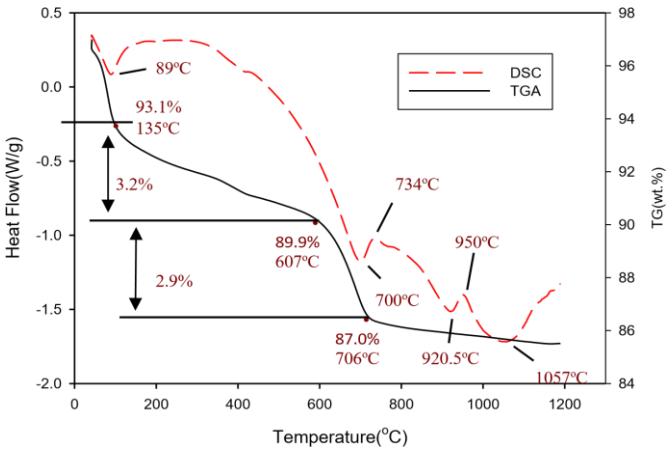

Figure 7. DSC and TGA analysis of the smectite (before being sintered at high temperatures)

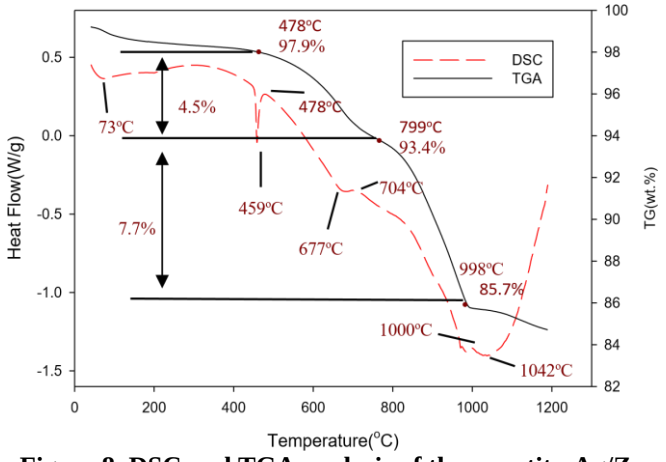

Figure 8. DSC and TGA analysis of the smectite-Ag/Zn

4. Discussion

This study used smectite clay as a carrier and exchanged Ag^{+} and Zn^{2+} onto the smectite via ion exchange. The coupled smectite-Ag/Zn catalysts at the nanolevel were formed after surface modification and high-temperature sintering. Various physicochemical experiments, such as Fourier-transform infrared spectroscopy (FT-IR) analysis, x-ray diffraction (XRD) analysis, transmission electron microscopy (TEM) analysis, and thermal analysis, were conducted to further discuss the physicochemical properties of the smectite-Ag/Zn.

In this study, an analysis on the modified smectite-Ag/Zn conducted via an FT-IR spectrum shows that the structure of the smectite-Ag/Zn remains intact; it still maintains the absorption band of clay minerals with inherent characteristics. A TEM observation of the coupled smectite-Ag/Zn catalysts after they were sintered at 350°C shows that the sizes of Ag^{+} and Zn^{+2} on the smectite-Ag/Zn are between 25-500 nm, respectively. This proves that the modified smectite-Ag/Zn catalysts are at the nanolevel. In terms of the thermal analysis, this study shows that endothermic peaks occur when the smectite is at 920°C and 1057°C, respectively. This means that the smectite is in the dissolving, not the amorphous, state. Also, significant melting occurs when the coupled smectiteAg/Zn catalysts are sintered at 459°C due to the oxidative pyrolysis of micromolecules or solvents. By the second pyrolysis, when the temperature reaches 998°C, weight loss seems to be quite obvious since the exothermic peak and melting and recrystallization phenomena are less obvious.

References

[1].Boxi, S.S., Paria, S. (2015). Visible light induced enhanced photocatalytic degradation of organic pollutants in aqueous media using Ag doped hollow TiO_2 nanospheres. RSC Advance 119, 37657.

[2].Chen, F., Yang, X., Xu, F., Wu, Q., and Zhang, Y. (2009). Correlation of photocatalytic bactericidal effect and organic matter degradation of TiO_2 part 1: observation of phenomena. Environ. Sci. Technol. 43, 1180.

[3].Fujishima, A., Honda, K. (1972). Electrochemical photolysis of water at a semiconductor electrode. Nature 238, 5358.

[4].Gordon, T. R., Cargnello, M., Paik, T., Mangolini, F., Weber, R.T., Fornasiero, P., Murray, C. B. (2012). Nonaqueous synthesis of TiO_2 nanocrystals using TiF4 to engineer morphology, oxygen vacancy concentration, and photocatalytic activity. Journal of the American Chemical Society 134, 6751.

[5].Kushwaha, H. S., Halder, A., Jain, D., Vaish, R. (2015). Visible light-induced photocatalytic and antibacterial activity of li-doped $Bi_{0.5}Na_{0.45}K_{0.5}TiO_3$–$BaTiO_3$ ferroelectric ceramics. Journal of Electronic Materials 44, 4334.

[6].Mo, J., Zhang, Y., Xu, Q., Lamson, J.J., and Zhao, R. (2009). Photocatalytic purification of volatile organic compounds in indoor air: a literature review. Atmos. Environ. 43, 2229.

[7].Paz, Y. (2010). Application of TiO_2 photocatalysis for air treatment: Patents' overview. Appl. Catal. B Environ. 99, 448.

[8].Pelaez, M., Nolan, N. T., Pillai, S. C., Seery, M. K., Falaras, P., Kontos, A. G., Dunlop, P. S. M., Hamilton, J. W. J., Byrne, J. A., O'Shea, K., Entezari, M.H., Dionysiou, D. D. (2012). A review on the visible light active titanium dioxide photocatalysts for environmental applications. Applied Catalysis B: Environmental 125, 331.

[9].Satoh, N., Nakashima, T., Kamikura, K., Yamamoto, K. (2008). Quantum size effect in TiO_2 nanoparticles prepared by finely controlled metal assembly on dendrimer templates. Nature Nanotechnology 3, 106.

[10]. Yang, H. G., Sun, C. H. Qiao, S. Z., Zou, J., Liu, G., Smith, S. C., Cheng, H.M., Lu, G. Q. (2008). Anatase TiO_2 single crystals with a large percentage of reactive facets. Nature 453, 638.

[11]. Salvad-Estivill, I., Hargreaves, D.M., and Puma, G.L. (2007). Evaluation of the intrinsic photocatalytic oxidation kinetics of indoor air pollutants. Environ. Sci. Technol. 41, 2028.

[12]. Sobana, N., Muruganandam, M., Swaminathan, M. (2008). Characterization of AC–ZnO catalyst and its photocatalytic activity on 4-acetylphenol degradation, Catal. Commun. 9, 262.

[13]. Xie, Y. J., Zhang, X., Ma, P. J., Wu, Z. J., Piao, L. Y.(2016). Mesoporous silicon carbide nanofibers with in situ embedded carbon for co-catalyst free photocatalytic hydrogen production. Nano Research 9, 886.

[14]. Zhang, F.J., Chen, M. L., Oh, W. C. (2009). Fabrication and electro-photolysis property of carbon nanotubes/titanium composite photocatalysts for methylene blue, Bull. Korean Chem. Soc. 30, 1798.

[15]. Zhong, L., Haghighat, F., Blondeau, P., and Kozinski, J. (2010). Modeling and physical interpretation of photocatalytic oxidationefficiencyinindoorair applications. Build. Environ. 45, 2689.